IEEE Access
Multidisciplinary | Rapid Review | Open Access Journal

Received March 19, 2021, accepted April 12, 2021, date of publication April 15, 2021, date of current version April 26, 2021.

Digital Object Identifier 10.1109/ACCESS.2021.3073488

Transceiver Design for Full-Duplex UAV Based Zero-Padded OFDM System With Physical Layer Security

JOARDER JAFOR SADIQUE[1], SHAIKH ENAYET ULLAH[2], MD. RABIUL ISLAM[3], (Senior Member, IEEE), RAAD RAAD[3], (Member, IEEE), ABBAS Z. KOUZANI[4], (Member, IEEE), AND M. A. PARVEZ MAHMUD[4]

[1]Department of Electrical and Electronic Engineering, Begum Rokeya University, Rangpur 5404, Bangladesh
[2]Department of Electrical and Electronic Engineering, University of Rajshahi, Rajshahi 6205, Bangladesh
[3]Faculty of Engineering and Information Sciences, University of Wollongong, Wollongong, NSW 2522, Australia
[4]School of Engineering, Deakin University, Geelong, VIC 3216, Australia

Corresponding author: Joarder Jafor Sadique (joarder@brur.ac.bd)

ABSTRACT In this paper, multi-antenna transceiver for zero-padded orthogonal frequency division multiplexing (OFDM) system is designed at mmWave by integrating full-duplex unmanned aerial vehicle (UAV) into the terrestrial cellular networks. Assuming that there exist no direct communication links between the ground base station (GBS) and the mobile users due to unexpected blockages from high storied buildings in urban area, the UAV applies decode-and-forward cooperative strategy on the received OFDM signals transmitted from GBS and re-transmits to the ground mobile users and passive eavesdropper. In this proposed system, intertwining logistic map (ILM)-cosine transform aided encryption algorithm combined with artificial noise enhancing physical layer security (PLS) is introduced. Also walsh-hadamard transform technique integrated with QR-decomposition based zero forcing (ZF) block diagonalization (QR-ZF-BD) precoding for multi-user interference reduction and non-iterative clipping and filtering technique for peak to average power ratio (PAPR) reduction are utilized. In addition, Low density parity check (LDPC) and repeat and accumulate (RA) channel coding with cholesky decomposition based ZF and minimum mean square error signal detection schemes for improved bit error rate (BER) are also introduced. Numerical results demonstrate the effectiveness of the proposed system in terms of PLS for color image transmission at high order digital modulation (16-PSK and 16-QAM). At the complementary cumulative distribution function of probability level 1-6%, the estimated PAPR is found to have value of 6 dB.The three users achieve BER $= 1 \times 10^{-4}$ at signal-to-noise ratio of 1.5 dB, 4 dB and 6 dB under RA channel coding and 16-QAM digital modulation.

INDEX TERMS Bit error rate, channel coding, peak to average power ratio, physical layer security encryption, signal-to-noise ratio, zero-padded orthogonal frequency division multiplexing.

I. INTRODUCTION

Owing to cost effectiveness and high mobility deployment flexibility, suitable use of unmanned aerial vehicles (UAVs) in wireless communication networks has grown enough interest within academia, government organization and research industries. UAVs have also been proposed for use in both logistical delivery of goods networks while concurrently supporting data connectivity functions [1]–[3]. UAV based wireless network is acknowledged as a promising technique to ensure proper communication link under natural and man-made disasters like floods, fires and earthquakes. With the flexibility, maneuverability and high chance of establishing line-of-sight (LOS) drone to-ground communications, the UAVs equipped with communication capabilities can be leveraged for information dissemination as well as coverage expansion of ground wireless and cellular networks. The UAVs are capable of assisting vehicle-to-vehicle (V2V) communications by disseminating safety and traffic messages among vehicles within a vehicular network and also

The associate editor coordinating the review of this manuscript and approving it for publication was Xueqin Jiang.

This work is licensed under a Creative Commons Attribution 4.0 License. For more information, see https://creativecommons.org/licenses/by/4.0/

facilitating fast and efficient information dissemination in device-to-device (D2D) communication networks as well as mobile ad-hoc networks. In next generation communication systems, full-duplex relaying scheme allowing simultaneous transmission and reception from a relay node and non-orthogonal multiple access (NOMA) power domain signaling technique have been considered as potential techniques to improve spectral efficiency [4], [5]. In UAV-assisted mmWave NOMA networks, a huge volume of secret messages are communicated within highly interrelated systems pose serious level of challenges on protected wireless communications and physical layer security (PLS). With proper utilization of multiple antennas, maximum ratio transmitting (MRT) beamforming and sending artificial noise (AN) to jam potential eavesdroppers (EVEs) may be considered as efficient ways to enhance physical layer security [6], [7].

Currently, the existing commercially deployed 5G new radio (NR) networks support internet-of-things (IoT), enhanced mobile broadband (eMBB) and multimedia-broadcast single frequency network (MBSFN) with NR OFDM numerology under the standardization of the 3rd generation partnership project (3GPP). The 5G new radio (NR) networks use both centimeter wave (cmWave) and millimeter wave (mmWave) radio frequencies (3.4 to 3.6 GHz below 6 GHz) and (24.25 to 27.5 GHz, 27.5 to 29.5 GHz, 37 GHz, 39 GHz and 57 to 71 GHz) [8], [9]. In continuation of further development of OFDM technology with consideration of improving PLS and compensation of interference due to multipath fading, much attention has been given on the zero-padded OFDM (ZP-OFDM) signaling. The ZP-OFDM has become a popular technique to provide excellent performance in the high-speed mobile channels with reduction of inter-carrier interference (ICI) and prevention of destroying orthogonality among subcarriers [10].

A. PRIOR WORKS

In order to provide on-request and stable wireless connectivity to planned areas, unmanned aerial vehicles (UAVs) have gained tremendous level of interest with a view to integrating the system with terrestrial wireless networks largely due to their strong line-of-sight (LOS) links, maneuverability and flexible/instant deployment. The authors of [11] presented uncoded bit error rate (BER) performance of index modulation (IM) aided multiple-mode (MM) orthogonal frequency division multiplexing (MM-OFDM-IM) system and highlighted its dominance in comparison with the conventional OFDM system. At [12], authors proposed a novel layered orthogonal frequency division multiplexing with index modulation (L-OFDM-IM) scheme to enhance the spectral efficiency (SE) of OFDM-IM systems along with coordinate interleaving L-OFDM-IM (CI-OFDM-IM) system in order to further improve the diversity performance of L-OFDM-IM. In their work, BER performance comparison between different forms of IM based layered OFDM scheme has been presented. The authors of [13] proposed OFDM with hybrid in-phase/quadrature index modulation (OFDM-HIQ-IM) and linear constellation precoded OFDM-IQ-IM (LP-OFDM-IQ-IM) to enhance SE as well as the BER performance of the OFDM-IM systems. In their works, BER performances of the OFDM-HIQ-IM and LP-OFDM-IQ-IM systems have been investigated in comparison with the classical OFDM as well as existing OFDM-IM schemes. In [14], the authors considered employing cellular-linked aerial user equipment (AUE) for surveillance and monitoring. They enabled AUE for continuous uplink transmissions and also utilized power-domain uplink aerial-terrestrial non-orthogonal multiple access (NOMA) enabling terrestrial user equipment (TUE). In their work, numerically extracted minimum height of AUE was used to achieve a certain quality of service (QoS) constraint for different AUE target data rates and built-up areas. The authors of [15] explored attributes of mobile self-organizing network containing several UAVs and targeted improving the communication link of UAV network. They developed a MIMO-OFDM communication system considering technical values and system models of multiple input multiple output (MIMO) and orthogonal frequency division multiplexing (OFDM) techniques. In their work, they also showed that the use of MIMO-OFDM technology in UAV communication network successfully enhanced the capability of data transmission. In [16], the authors proposed OFDM-assisted unmanned aerial vehicle (UAV) communication system utilizing a deep learning based channel along with carrier frequency offset (CFO) equalization technique. They claimed that the performance of their proposed scheme was better than the existing schemes and also valid under several propagation environments.

B. CONTRIBUTION AND ORGANIZATION

The key contribution of this paper is the designing of a multi-antenna transceiver for a full-duplex UAV-assisted terrestrial cooperative zero-padded OFDM system utilizing various significant components. From the state of the art, it has been observed that various individual multicarrier-signaling techniques such as, non-orthogonal multiple access (NOMA), generalized frequency division multiplexing (GFDM), universal filtered multicarrier (UFMC), filter bank multicarrier (FBMC) etc were previously considered as excellent candidate waveform for 5G. At present, it is seen that multiple numerology supported OFDM-based signaling techniques (CP-OFDM and DFT-s-OFDM) have gained much popularity among the researchers of 5G New Radio (NR) networks. The major contributions of the paper are outlined as follows-

- In order to reduce the computational complexity of a precoding technique, QR decomposition based zero forcing (ZF) block diagonalization (QR-ZF-BD) precoding scheme combined with complex hadamard transform for multi-user interference (MUI) reduction is proposed.
- With the aim of compensating multipath fading channel effect and reducing peak to average power ratio (PAPR), properly designed subcarrier mapping with zero padding

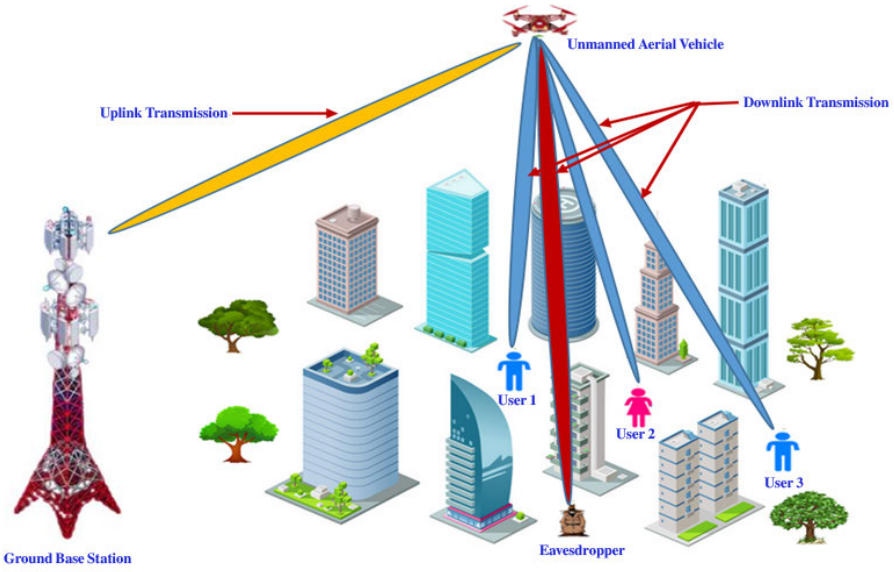

FIGURE 1. Scenario of full-duplex UAV based zero-padded OFDM system at mmWave.

with application of non-iterative clipping and filtering technique are proposed.

- Dua *et al.*'s proposed algorithm [17] of an anti-eavesdropping cryptographic technique and artificial-noise-aided signaling of power allocation [18] are introduced in this proposed system for PLS encryption.
- Simulation results verify the significant enhancement of PLS by making the channel of eavesdropper (Eve) noisier than the channels of valid users. It also illustrates acceptable bit error rate (BER) performance and PAPR reduction.

In general, block diagonalization (BD) is a well-known linear precoding scheme which usually provides good performance for MUI reduction. But in such scheme, high computational complexity arises due to two singular value decomposition (SVD) operations for each user. That's why QR-ZF-BD precoding scheme is proposed in this work. To the best of authors' knowledge, designing such UAV-enabled zero-padded OFDM system in multi-user environment is largely unexplored. The rest of this paper is organized as follows. In section II, the system model of our proposed mmWave UAV-assisted terrestrial cooperative zero-padded OFDM system is introduced including network description, block diagram and signal model. Simulation and Numerical results are presented and discussed in section III. Finally, section IV provides a brief summary and concluding remarks with future challenges. Throughout the paper, the notations $(.)^T$, $(.)^H$ and $||.||^2$ denote transpose, Hermitian transpose and square of Euclidian norm of matrix operation respectively and E(.) is the expectation operator.

II. SYSTEM MODEL

A. SCENARIO DESCRIPTIONS

A scenario of mmWave signal transmission is presented in Figure 1 for zero-padded OFDM signaling based unmanned aerial vehicle (UAV) integrated terrestrial wireless network. In such downlink UAV integrated terrestrial cellular networking, one ground base station, one UAV, three ground users and a passive eavesdropper are considered with each is equipped with multiple antennas. As a full-duplex (FD) relay transmission protocol, decode-and-forward (DF) strategy is adopted to help data transmission between the base station and the users [4]. DF relaying strategy is preferred in comparison to another promising FD transmission protocol, amplify-and-forward (AF) considering the impact of realistic UAV channel models introduced at [19]. Here, a UAV channel model is considered and tested across multiple signal-to-noise ratio (SNR) scenarios. An optimum adaption of SNR for multiple users for the system associated with a single UAV is proposed. Also, some special type of communication strategy is adopted to meet up the key challenges associated with compensation of multipath fading channel effect and severe path loss with blockage in mmWave signal transmission.

B. BLOCK DIAGRAM

The conceptual block diagram of the full-duplex UAV-assisted zero-padded OFDM system is shown in Figure 2. Figure 2 shows that three users are assumed to receive their own transmitted data in the form of color image and with the significant reduction of user's signal leakage, the passive eavesdropper would receive merely noisy data. The pixel values of the three red, green and blue components of each individual user's color image are encrypted with improved intertwining logistic map (ILM)-cosine transform-based cryptographic technique [17] and the extracted binary data are first sent up through the channel encoder followed by digital modulator to generate the complex symbols [20]–[22] and subsequently spread out for symbol copying using walsh-hadamard transform (WHT) technique [23]. In each

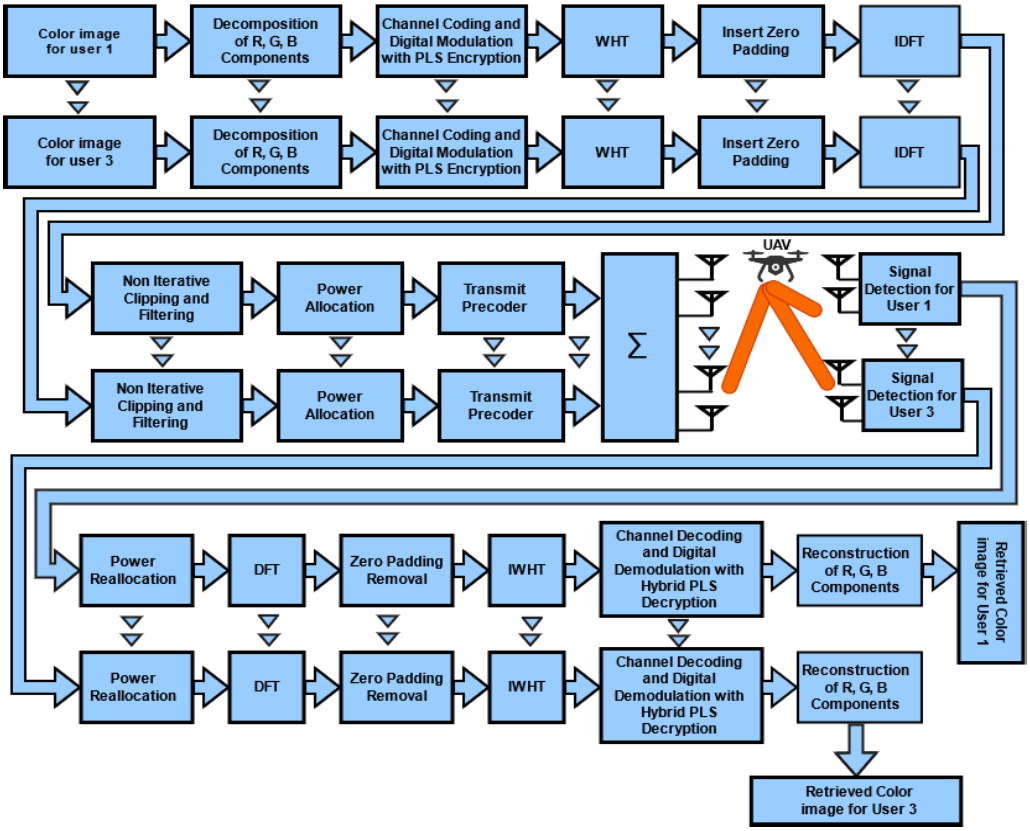

FIGURE 2. Block diagram of full-duplex UAV-assisted terrestrial cooperative zero-padded OFDM system.

zero-padded OFDM symbol, the WHT encoded complex symbols are mapped into the desired number of subcarriers in the frequency bandwidth and the null subcarriers (zero-paddings) are added at both ends of the data subcarriers [10]. The zero-padded OFDM signals are oversampled and processed with clipping and filtering technique under consideration of targeted PAPR value [24]. The clipped and filtered signals of the three users in addition to artificially generated noisy signal for an passive eavesdropper are precoded with channel dependent transmit precoding schemes [25] after power scaling and the baseband equivalent spatially-multiplexed signals are transmitted from ground base station to unmanned aerial vehicle. At the receiving end of each user, linear signal detection scheme, cholesky decomposition (CD) based ZF/minimum mean square error (MMSE) is used to detect all the transmitted signals [26], [27]. The detected signal is power scaled, OFDM demodulated with removing padded zeros and despreaded through multiplying with inverse WHT technique. The despreaded signal will pass through digital demodulator, channel decoder and further process with PLS decryption technique to retrieve color image from its reconstructed red, green and blue components.

C. SIGNAL MODEL

In this proposed system, the ground base station is considered to be composed of N_T (=8) transmitting antennas, each of the three ground users and a passive eavesdropper are equipped with N_R (=2) receiving antennas and the UAV is of $N_T \times N_T$ MIMO antenna configured. With giving emphasis on PLS, an improved cosine transformed based 3-D intertwining logistic map (ILM) encryption technique addressed in [17] with modified parameters has been considered to represent the complex chaotic sequences for the user k in i^{th} times of iterations as:

$$x_{k,i+1} = \cos([\lambda_k \times l_k \times y_{k,i} \times (1 - x_{k,i}) + z_{k,i}] mod 1 + \beta_k) \quad (1a)$$

$$y_{k,i+1} = \cos([\lambda_k \times \beta_k \times y_{k,i} + z_{k,i} \times (1 + x_{k,i+1}^2)] mod 1 + \beta_k) \quad (1b)$$

$$z_{k,i+1} = \cos([\lambda_k \times (y_{k,i+1} + x_{k,i+1} + \gamma_k) \times \sin(z_{k,i})] mod 1 + \beta_k) \quad (1c)$$

where the values of parameters used in (1a)-(1c) for three users (k = 1, 1, 3) are:

λ_k = [1.5 2.5 3.5], l_k = [34.5 35.5 36.5], $x_{k,0}$ = [0.1 0.2 0.3], $y_{k,0}$ = [0.4 0.5 0.6], $z_{k,0}$ = [0.7 0.8 0.9] and β_k = [38.1 39.1 40.1]. The chaotic sequence of (1c) is considered with its application to the red, green and blue components of each of the three user's color image and mapped into integer sequence (0-255)/encrypted keys for a total number of pixel points in each color image component N (i = 1, 2, 3 . . . N).

The encrypted keys for color image components of three users can be written as:

$$K_1 = mod(round(z_{1,i} \times \lambda_{11}), 256) \quad (2a)$$
$$K_2 = mod(round(z_{2,i} \times \lambda_{22}), 256) \quad (2b)$$
$$K_3 = mod(round(z_{3,i} \times \lambda_{33}), 256) \quad (2c)$$

where $\lambda_{11} = 0.5 \times 10^9$, $\lambda_{22} = 1.0 \times 10^9$ and $\lambda_{33} = 1.5 \times 10^9$. Using pixel wise XOR operation between each color image component of individual user with assigned keys presented in (2a)-(2c), modified form of cosine transformed ILM based encrypted color image are formed. With extracting all binary data from encrypted color image, the binary bit sequence for the user k of data length $\ddot{N}$ can be shown as:

$$b_k = [b_{k,1}, b_{k,2}, \ldots\ldots\ldots\ldots b_{k,\ddot{N}}] \quad (3)$$

The binary data vector $\mathbf{b_k}$ is channel encoded to form a new binary data vector $\mathbf{c_k}$ of data length N and the $\mathbf{c_k}$ is further converted into digitally modulated complex symbol vector $\mathbf{x_k}$ with data length $\bar{N}$. The signal vector $\mathbf{x_k}$ is spreaded through multiplying with one dimensional discrete WHT matrix of order 8, $\mathbf{W_{k,r}}$ which is addressed in [23]. In 8×8 sized $\mathbf{W_{k,r}}$ WHT matrix, rth rows (r = 2, 3, 4) are chosen for the three users and 5^{th} row ($\bar{r} = 5$) is chosen for the eavesdropper and its digitally modulated complex symbol vector $\bar{\mathbf{x}}_{\mathbf{eve}}$ of data length $\bar{N}$ (originated from artificially generated binary data of length $\ddot{N}$). The WHT signal for the user k can also be shown as:

$$\ddot{\mathbf{x}}_{\mathbf{k}} = \mathbf{W_{k,r}} \mathbf{x_k} \quad (4)$$

where $\ddot{\mathbf{X}}_k$ is of data length $\tilde{N}$. In case of eavesdropper with identical data length, the WHT signal can be written as:

$$\ddot{\mathbf{X}}_{\mathbf{eve}} = \mathbf{W_{k,\bar{r}}} \bar{\mathbf{x}}_{\mathbf{eve}} \quad (5)$$

The data symbol vector $\ddot{\mathbf{X}}_{\mathbf{k}}$ for the user k is transformed into matrix $\tilde{\mathbf{X}}_{\mathbf{k}}$ of a size $\widehat{N} \times L$, where L is the number of zero padded OFDM symbols, $\widehat{N}$(=3300) is the number of data subcarriers. The data symbol vector $\ddot{\mathbf{X}}_{\mathbf{eve}}$ for the eavesdropper is also transformed into matrix $\tilde{\mathbf{X}}_{\mathbf{eve}}$ of identical size. Prior to producing discrete-time domain OFDM symbol with zero padding of data length N(=4096) for both user k and eavesdropper, the null subcarriers of sample length $\overrightarrow{N} = 0.5(N - \widehat{N})$ are added to both the ends of $\widehat{N}$ data subcarriers to the each column data vector of matrices $\tilde{X}_k$ and $\tilde{X}_{eve}$ to form properly designed sub carrier mapped input data matrices X_k and X_{eve} each of which of size $N \times L$. The *lth* discrete-time domain zero padded OFDM symbol for *mth* time-domain sample index and *nth* subcarrier for user k and eavesdropper can be written as [10]:

$$\bar{X}_{k,l}[m] = \frac{1}{\sqrt{N}} \sum_{n=-\frac{N}{2}}^{\frac{N}{2}-1} X_{k,l}[n] e^{-\frac{j2\pi mn}{N}} \quad (6a)$$

$$\bar{X}_{eve,l}[m] = \frac{1}{\sqrt{N}} \sum_{n=-\frac{N}{2}}^{\frac{N}{2}-1} \bar{X}_{eve,l}[n] e^{-\frac{j2\pi mn}{N}} \quad (6b)$$

where the time-domain sample index, $m = 0, 1, 2, \ldots$. $(N-1)$ and the subcarrier index, n ranges from $-\frac{N}{2}$ to $\frac{N}{2} - 1$. The signal models presented in (6a) and (6b) are oversampled with an oversampling factor of $N_{ov}(= 4)$ through adding zeros of length $N_{add}(= 1.5N)$ at its both end to form new signal vectors $\widehat{\mathbf{X}}_{\mathbf{k,l}}[\bar{m}]$ and $\widehat{\mathbf{X}}_{\mathbf{eve,l}}[\bar{m}]$ of sample length $N_m = (NN_{ov})$, where $\bar{m}$ signifies time-domain sample index inside the oversampled OFDM symbol for the user k and the eavesdropper viz. $\bar{m} = 0, 1, 2, \ldots\ldots\ldots(N_m - 1)$. The PAPR for the signal vectors $\widehat{\mathbf{X}}_{\mathbf{k,l}}[\bar{m}]$ and $\widehat{\mathbf{X}}_{\mathbf{eve,l}}[\bar{m}]$ can be defined as:

$$PAPR(\widehat{X}_{k,l}) = \log_{10} \frac{max_{\bar{m}=0,1,2,3,\ldots N_m-1} |\widehat{X}_{k,l}[\bar{m}]|^2}{\frac{1}{N_m} \sum_{\bar{m}=0}^{N_m-1} |\widehat{X}_{k,l}[\bar{m}]|^2} \quad (7a)$$

$$PAPR(\widehat{X}_{eve,l}) = \log_{10} \frac{max_{\bar{m}=0,1,2,3,\ldots N_m-1} |\widehat{X}_{eve,l}[\bar{m}]|^2}{\frac{1}{N_m} \sum_{\bar{m}=0}^{N_m-1} |\widehat{X}_{eve,l}[\bar{m}]|^2} \quad (7b)$$

where $max_{(.)}\{.\}$ is the maximum operator and $\widehat{X}_{k,l}[\bar{m}]$ and $\widehat{X}_{eve,l}[\bar{m}]$ are the $\bar{m}$th sample of $\widehat{X}_{k,l}$ and $\widehat{X}_{eve,l}$. In non-iterative clipping and filtering technique to minimize PAPR, the PAPR target has been denoted by λ_{target}($\lambda_{target,dB}$ is its value in dB scale). On executing soft limiting based non iterative clipping operation, the clipped signal vectors for the user k and eavesdropper can be defined as:

$$\overleftrightarrow{X}_{k,l}[\bar{m}] = \begin{Bmatrix} A_0 e^{j\angle \widehat{X}_{k,l}[\bar{m}]}, & \text{if } \widehat{X}_{k,l}[\bar{m}] > A_0 \\ \widehat{X}_{k,l}[\bar{m}], & \text{otherwise} \end{Bmatrix} \quad (8a)$$

$$\overleftrightarrow{X}_{eve,l}[\bar{m}] = \begin{Bmatrix} A_{0eve} e^{j\angle \widehat{X}_{eve,l}[\bar{m}]}, & \text{if } \widehat{X}_{eve,l}[\bar{m}] > A_0 \\ \widehat{X}_{eve,l}[\bar{m}], & \text{otherwise} \end{Bmatrix} \quad (8b)$$

where $\left\{\angle \widehat{X}_{k,l}[\bar{m}] \text{ and} |\widehat{X}_{k,l}[\bar{m}]|\right\}$ and $\left\{\angle \widehat{X}_{eve,l}[\bar{m}] \text{ and.}\right\}$. $\left\{|\widehat{X}_{eve,l}[\bar{m}]|\right\}$ represents the phase angle and modulus of $\bar{m}$th complex number of signal vectors $\widehat{\mathbf{X}}_{k,l}$ and $\bar{\bar{\mathbf{X}}}_{eve,l}$ respectively. The amplitude threshold values A_{0k} and A_{0eve} can be computed as:

$$A_{0k} = \sqrt{\lambda_{target} E|\widehat{X}_{k,l}|^2} \quad (9a)$$

$$A_{0eve} = \sqrt{\lambda_{target} E|\widehat{X}_{eve,l}|^2} \quad (9b)$$

The clipped signals presented in (8a) and (8b) are converted into frequency-domain signals to suppress the clipping noise by computation of DFT of size N_m and further processed to reconvert into time domain signals $\overleftrightarrow{X}_{k,l}[\bar{m}]$ and $\overleftrightarrow{X}_{eve,l}[\bar{m}]$ [24]. The l^{th} discrete-time domain processed signal vectors $\overleftrightarrow{X}_{k,l}[\bar{m}]$ and $\overleftrightarrow{X}_{eve,l}[\bar{m}]$ for the user k and eavesdropper are rescaled such that $E|\overleftrightarrow{X}_{k,l}|^2 = 1$ and $E|\overleftrightarrow{X}_{eve,l}|^2 = 1$.The power rescaled signal vectors of unity power are represented by $\overrightarrow{X}_{k,l}[\bar{m}]$ and $\overrightarrow{X}_{eve,l}[\bar{m}]$. If identical signal power P is assigned to each user and $P_e(= \xi P)$ is assigned to the eavesdropper where ξ is the fraction of the allocated power P, the new signal vectors can be expressed as $\sqrt{P}\overrightarrow{X}_{k,l}[\bar{m}]$ and $\sqrt{P_e}\overrightarrow{X}_{eve,l}[\bar{m}]$. On concatenating all the signal vectors with consideration of oversampled zero padded OFDM symbols, the desired signals for the user k and eavesdropper can be represented by matrices S_k and S_e with each

of which is of $N_m \times L$ in size. Stacking all the elements of the matrixed data into single column vector and further converted into matrices of size $N_R \times N_S$, where $N_s = (N_m.L)/N_R$ and the input signals prior to processing with transmit precoding techniques for the user k and eavesdropper with matrix size $N_R \times N_S$ are:

$$S_{ko} = \sqrt{P} s_k \tag{10a}$$
$$S_e = \sqrt{P_e} s_e \tag{10b}$$

In designing transmit precoder, probabilistic path loss model based 3D geometrical MIMO fading channels have been considered for ground base station to unmanned aerial vehicle (UAV) and UAV to ground communications. The LOS probability can be written as:

$$P_{LOS}^{ij} = \frac{1}{1 + \psi exp(-\beta[\theta_{ij} - \psi])} \tag{11}$$

where $\psi(=11.95)$ and $\beta(=0.14)$ are a function of the carrier frequency and environment, θ_{ij} represents the elevation angle and $\theta = \frac{180}{\pi} \times sin^{-1}\frac{h_j^{uav} - h_i}{d_{ij}}$, where $d_{ij} = \sqrt{(x_i - x_j^{uav})^2 + (y_i - y_j^{uav})^2 + (h_i - h_j^{uav})^2}$ is the 3D distance between UAV **j** and the ground base station/ground user/eavesdropper **i** with $[x_j^{uav}, y_j^{uav}, h_j^{uav}]$ and $[x_i, y_i, h_i]$ are their 3D coordinates respectively. The path loss between the ground base station/ground user/eavesdropper and the UAV can be written as:

$$L_{ij} = \left\{ \begin{array}{l} \eta_1 \left(\frac{4\pi f_c d_{ij}}{c}\right)^{\alpha}, \text{ LOS Link} \\ \eta_2 \left(\frac{4\pi f_c d_{ij}}{c}\right)^{\alpha}, \text{ NLOS Link} \end{array} \right\} \tag{12}$$

where $\alpha(=2.0)$ is the path loss exponent, $f_c(=28GHz)$ is the carrier frequency, $\eta_1(=10^{3/10})$ and $\eta_2(=10^{23/10})$ are the excessive path loss coefficients for LOS and NLOS links and $c(=3 \times 10^8)$m/s is the light's speed. The NLOS probability is simply $P_{NLOS}^{ij} = 1 - P_{LOS}^{ij}$. The average path loss between the ground base station/ground user/eavesdropper and UAV can be written as:

$$\bar{L}_{ij} = P_{LOS}^{ij} \eta_1 \left(\frac{4\pi f_c d_{ij}}{c}\right)^{\alpha} + P_{NLOS}^{ij} \eta_2 \left(\frac{4\pi f_c d_{ij}}{c}\right)^{\alpha} \tag{13}$$

In case of uplink transmission from ground base station to UAV, the path loss L_0 for MIMO flat fading channel H_0 can be written as:

$$L_0 = P_{LOS}^{ij} \eta_1 \left(\frac{4\pi f_c d_{ij}}{c}\right)^{\alpha} \tag{14}$$

In case of downlink transmission from UAV to ground user/eavesdropper, the path loss L_k/L_e for k-th user's/eavesdropper's MIMO flat fading channel H_k/H_e can be written as:

$$L_k = P_{LOS}^{ij} \eta_1 \left(\frac{4\pi f_c d_{ij}}{c}\right)^{\alpha} + P_{NLOS}^{ij} \eta_2 \left(\frac{4\pi f_c d_{ij}}{c}\right)^{\alpha} \tag{15a}$$
$$L_e = P_{LOS}^{ij} \eta_1 \left(\frac{4\pi f_c \bar{d}_{ij}}{c}\right)^{\alpha} + P_{NLOS}^{ij} \eta_2 \left(\frac{4\pi f_c \bar{d}_{ij}}{c}\right)^{\alpha} \tag{15b}$$

where d_{ij} and $\bar{d}_{ij}$ are the 3D distances between the UAV and k-th user ($k = 1, 2, 3$) and the UAV and eavesdropper respectively [5]. On the basis of signal model presented in (14) through (15b), MIMO flat fading channel, H_0, H_1, H_2, H_3 and H_e are estimated. The H_1, H_2, H_3 and H_e are of each $N_R \times N_T$ and H_0 is of $N_R \times N_T$ matrix in size and are used to design transmit precoders for three users and eavesdropper with implementation of QR-BD Precoding algorithm [25]. The total MIMO channel matrix $H_s \mathbb{C}^{KN_R \times N_T}$ for a total number of users K is formulated as:

$$H_s = [H_1^T \; H_2^T \; H_3^T \ldots\ldots\ldots H_K^T]^T \tag{16}$$

The total channel matrix $\tilde{H}_k$ excluding the k-th user's channel can be written as:

$$\tilde{H}_s = [H_1^T \ldots H_{k-1}^T \; H_{k+1}^T \ldots\ldots H_K^T]^T \tag{17}$$

where $\tilde{H}_k \epsilon \mathbb{C}^{\tilde{N}_K \times N_T}$ and $\tilde{N}_k = N_T - 2 \times N_R$. For the case of QR-BD precoding algorithm, the pseudo-inverse of the matrix of $\tilde{H}_k$ for each user can be written as:

$$\tilde{H}_k^{\cdot\cdot} = \tilde{H}_k^H (\tilde{H}_k \tilde{H}_k^H)^{-1} \tag{18}$$

where $\tilde{H}_k^{\cdot\cdot} \epsilon \mathbb{C}^{N_T \times \tilde{N}_k}$ and on implementing QR decomposition on the matrix $(I_{N_T} - \tilde{H}_k^{\cdot\cdot} \tilde{H}_k)$ as:

$$I_{N_T} - \tilde{H}_k^{\cdot\cdot} \tilde{H}_k = Q_k R_k = [Q_k^1 \;\; Q_k^2] \begin{bmatrix} R_k^1 \\ 0 \end{bmatrix} \tag{19}$$

where I_{N_T} is the identity matrix of $N_T \times N_T$ in size, $R_k^1 \epsilon \mathbb{C}^{\tilde{N}_k \times N_T}$ is an upper triangular matrix, $Q_k^1 \epsilon \mathbb{C}^{N_T \times \tilde{N}_k}$ is an orthogonal matrix whose columns form an orthonormal basis for the matrix $(I_{N_T} - \tilde{H}_k^{\cdot\cdot} \tilde{H}_k)$. As $\tilde{H}_k (I_{N_T} - \tilde{H}_k^{\cdot\cdot} \tilde{H}_k) = 0$ and $Q_k^1 \epsilon \mathbb{C}^{N_T \times \tilde{N}_k}$ forms an orthogonal basis for the null space of $\tilde{H}_k$, Q_k^1 can be considered as the QR-BD precoded matrix W_k for user k viz.

$$W_k = Q_k^1 \tag{20}$$

In case of estimating QR-BD precoded matrix W_e for a passive eavesdropper, the total channel matrix $\tilde{\tilde{H}}_e$ excluding the eavesdropper's channel is identical as presented in (16). Again for the case of QR-BD precoding algorithm, the pseudo-inverse of the matrix of $\tilde{\tilde{H}}_e$ for eavesdropper can be written as:

$$\tilde{\tilde{H}}_e^{\cdot\cdot} = \tilde{\tilde{H}}_e^H (\tilde{\tilde{H}}_e \tilde{\tilde{H}}_e^H)^{-1} \tag{21}$$

where $\tilde{\tilde{H}}_e^{\cdot\cdot} \epsilon \mathbb{C}^{N_T \times N_T}$ and on implementing QR decomposition on the matrix $(I_{N_T} - \tilde{\tilde{H}}_e^{\cdot\cdot} \tilde{\tilde{H}}_e)$ as:

$$I_{N_T} - \tilde{\tilde{H}}_e^{\cdot\cdot} \tilde{\tilde{H}}_e = Q_e R_e = [Q_e^1 \;\; Q_e^2] \begin{bmatrix} R_e^1 \\ 0 \end{bmatrix} \tag{22}$$

In (22), $Q_e^1 \epsilon \mathbb{C}^{N_T \times N_R}$ would form an orthogonal basis for the null space of $\tilde{\tilde{H}}_e$ and Q_e^1 can be considered as the QR-BD precoded matrix W_e for eavesdropper [25] viz.

$$W_e = Q_e^1 \tag{23}$$

Using signal models of (10a) and (10b), considering estimated precoded matrices, the transmitted precoded signal from ground base station to UAV can be written as:

$$X = \sum_{k=1}^{k=K} W_k\sqrt{P}s_k + W_e\sqrt{P_e}s_e \tag{24}$$

The signal received at the UAV can be represented as:

$$\begin{aligned} Y &= H_0X + n_{uav} \\ &= H_0\sum_{k=1}^{k=K} W_k\sqrt{P}s_k + W_e\sqrt{P_e}s_e + n_{uav} \end{aligned} \tag{25}$$

where $n_{uav} \sim \mathbb{CN}(0_{N_T}, \sigma_n^2 I_{N_T})$ denotes the additive white Gaussian noise (AWGN).With application of cholesky decomposition (CD) based ZF signal detection technique addressed at [26], the transmitted signal X can be decoded from (25). Multiplying (25) by $(H_0^H H_0)^{-1}H_0^H$, it can be calculated as-

$$\begin{aligned} S &= (H_0^H H_0)^{-1}H_0{}^H Y \\ &= (H_0^H H_0)^{-1}H_0{}^H H_0\left\{\sum_{k=1}^{k=K} W_k\sqrt{P}s_k + W_e\sqrt{P_e}s_e\right\} \\ &\quad + (H_0^H H_0)^{-1}H_0{}^H n_{uav} \end{aligned} \tag{26}$$

On Cholesky decomposition of matrix $(H_0^H H_0)$ into matrix $(L_0 L_0^H)$, where L_0 is the lower triangular matrix, (26) can be written in modified form as:

$$\begin{aligned} \tilde{S} &= (L_0L_0^H)^{-1}H_0{}^H Y \\ &= (L_0L_0^H)^{-1}H_0{}^H H_0\left\{\sum_{k=1}^{k=K} W_k\sqrt{P}s_k + W_e\sqrt{P_e}s_e\right\} \\ &\quad + (L_0L_0^H)^{-1}H_0{}^H n_{uav} \\ &= \left\{\sum_{k=1}^{k=K} W_k\sqrt{P}s_k + W_e\sqrt{P_e}s_e\right\} + \bar{n}_{uav} \end{aligned} \tag{27}$$

where $(L_0^{-H}L_0^{-1})H_0{}^H H_0$ is of $N_T \times N_T$ identity matrix and $\bar{n}_{uav} = (L_0L_0^H)^{-1}H_0{}^H n_{uav} \sim \mathbb{CN}(0_{N_T}, \sigma_n^2 I_{N_T})$ is a modified form of AWGN noise vector. Neglecting the noise component in (27) as compared to second bracketed desired signal, the detected signal $\bar{S}$ with CD based ZF signal detection technique can be written as:

$$\bar{S} = \sum_{k=1}^{k=K} W_k\sqrt{P}\bar{s}_k + W_e\sqrt{P_e}\bar{s}_e \tag{28}$$

In case of applicability of minimum mean square error (MMSE) signal detection technique [27] to (25), the detected signal $\tilde{S}$ with MMSE signal detection technique can be written as:

$$\tilde{S} = (H_0^T H_0 + \sigma_n^2 I)^{-1}H_0^T Y \tag{29}$$

where σ_n^2 denotes noise variance of the additive white Gaussian noise (AWGN). The signal presented in (28)/(29) will be sent up from the UAV to the ground users and eavesdropper. In case of CD based ZF detected signal, the signal received at user k can be written as:

$$Y_k = H_kW_k\sqrt{P}\bar{s}_k + \sum_{i=1,i\neq k}^{i=K} H_kW_i\sqrt{P}\bar{s}_i + H_kW_e\sqrt{P_e}\bar{s}_e + n_k \tag{30}$$

where $n_k \sim \mathbb{CN}(0_{N_R}, \sigma_n^2 I_{N_R})$ is the AWGN noise at the user k. In case of the wiretapped signal received at the Eavesdropper, it can be written as:

$$Y_{ev} = \sum_{k=1}^{k=K} H_eW_k\sqrt{P}\bar{s}_i + H_eW_e\sqrt{P_e}\bar{s}_e + n_e \tag{31}$$

where $\tilde{n}_e \sim \mathbb{CN}(0_{N_R}, \sigma_e^2 I_{N_R})$ is the AWGN noise at the eavesdropper. In (31) the value of H_eW_k is negligible and the eavesdropper would virtually receive noisy signal.

In (30), $||H_kW_k\sqrt{P}||^2$ is the instantaneous total power of the desired signal for user k, $||H_kW_i\sqrt{P}||^2$ is the instantaneous total interference power of the i-th users on the signal received by the user k, $||H_kW_e\sqrt{P_e}||^2$ is the additional instantaneous total interference power of the eavesdropper on the signal received by the user k respectively. As the signal model of (30) contains undesired signal obtained as the sum of noise and interference signal, the received signal-to-interference-noise ratio for the user k ($SINR_k$) can be written as:

$$SINR_k = \frac{||H_kW_k\sqrt{P}||^2}{N_R\sigma_n^2 + \sum_{i=1,i\neq k}^{i=K}||H_kW_i\sqrt{P}||^2 + ||H_kW_e\sqrt{P_e}||^2} \tag{32}$$

Considering (30) and (31), the received signal-to-interference-noise ratio for the eavesdropper ($SINR_{ev}$) can be written as:

$$SINR_{ev} = \frac{||H_kW_e\sqrt{P_e}||^2}{N_R\sigma_e^2 + \sum_{k=1}^{k=K}||H_kW_k\sqrt{P}||^2} \tag{33}$$

The achievable ergodic rate R_k for user k is a logarithmic function of signal-to-interference-noise ratio and it can be written as:

$$\begin{aligned} R_k &= \mathbb{E}\{log_2(1 + SINR_k)\} \\ &= \mathbb{E}\left\{\log_2(1 \right. \\ &\quad \left. + \frac{||H_kW_k\sqrt{P}||^2}{N_R\sigma_n^2 + \sum_{i=1,i\neq k}^{i=K}||H_kW_i\sqrt{P}||^2 + ||H_kW_e\sqrt{P_e}||^2}\right\} \end{aligned} \tag{34}$$

The achievable secrecy rate of the user k in case of CD based ZF detected signal can be written as:

$$R_k^{sec} = \left\{\log_2(1 + SINR_k) - \log_2(1 + SINR_{ev})\right\}^+ \tag{35}$$

where $\{x\}^+ = max(0, x)$ [28]–[30]

However, in order to formulate the analytical expression to characterize the proposed system in terms of achievable ergodic rate/ achievable ergodic spectral efficiency and

achievable secrecy rate using (30) and (31), the signal model introduced in (30) can be presented in its simplified form excluding its own channel matrix due to the fact that the computed precoding matrix forms an orthonormal basis for the null space of the total channel matrix. Now, neglecting the values of the $H_k W_i$ and $H_k W_e$, (30) can be written as:

$$\bar{Y}_k = H_k W_k \sqrt{P}\bar{s}_k + n_k = \overline{\overline{H}}_k \sqrt{P}\bar{s}_k + n_k \tag{36}$$

where $\overline{\overline{H}}_k = H_k W_k$ represents equivalent channel matrix for user k. Using CD based ZF signal detection technique to (36) and subsequent power rescaling, the user's own signal $\bar{\bar{s}}_k$ can be detected. In case of MMSE detected signal, the signal received at user k can be written as:

$$\tilde{Y}_k = H_k W_k \sqrt{P}\tilde{s}_k + \sum_{i=1, i\neq k}^{i=K} H_k W_i \sqrt{P}\tilde{s}_i + H_k W_e \sqrt{P_e}\tilde{s}_e + \tilde{n}_k \tag{37}$$

where $\tilde{n}_k \sim \mathbb{CN}(0_{N_R}, \sigma_{\tilde{n}^2} I_{N_R})$ denotes AWGN noise at the user k. Considering both W_i and W_e are orthonormal basis for zero space of H_k, viz. $H_k W_i = 0$ and $H_k W_e = 0$, (37) can be written in its simplified form as:

$$\tilde{\tilde{Y}}_k = H_k W_k \sqrt{P}\tilde{s}_k + \tilde{n}_k = \overline{\overline{H}}_k \sqrt{P}\tilde{s}_k + \tilde{n}_k \tag{38}$$

where $\overline{\overline{H}}_k = H_k W_k$ is the equivalent channel matrix for user k. Using MMSE signal detection technique to (38) and subsequent power rescaling, the user's own signal $\tilde{\tilde{s}}_k$ can be detected. In case of the wiretapped signal received at the Eavesdropper on the basis of MMSE detected signal, it can be written as:

$$\tilde{Y}_{ev} = \sum_{k=1}^{k=K} H_e W_k \sqrt{P}\tilde{s}_i + H_e W_e \sqrt{P_e}\tilde{s}_e + \tilde{n}_e \tag{39}$$

where $\tilde{n}_e \sim \mathbb{CN}(0_{N_R}, \sigma_{\tilde{e}}^2 I_{N_R})$ is the AWGN noise at the eavesdropper. In (39) the value of $H_e W_k$ is negligible and the eavesdropper would virtually receive noisy signal.

III. SIMULATION AND NUMERICAL RESULTS

In this part, numerical results are presented and analyzed for full-duplex UAV based Zero-padded OFDM System processed under the simulation parameters presented in Table 1. Here, a special case of three users and a passive eavesdropper is considered who are located at a distance of 67 m, 81 m, 145 m and 147 m from ground base station and the distance between ground base station and UAV is 180 m. In this study, it is assumed that the locations of the high mobility UAV, three ground users and the eavesdropper are well known to everyone. The channel state information (CSI) is generally needed to be estimated at the ground users and eavesdropper. Practically, the transmitting UAV and ground receiver (user/eavesdropper) can have different CSI. In this case, probabilistic path loss model addressed at [5] is considered and CSI can be obtained in specific cases of downlink transmission from the estimated MIMO flat fading channel. Such estimated channels are used both in transmit precoding at transmitter side and in channel equalization/signal detection at receiver side.

TABLE 1. Simulation parameters.

Description	Value
Size of color image (pixels)	$240 \times 180 \times 3$
mmWave carrier frequency (GHz)	28
Nominal OFDM transform size	4096
No. of active subcarriers	3300
Oversampling factor	4
Oversampled inverse discrete fourier transform (IDFT) size	4×4096
UAV height (m)	200
Ground base station height (m)	50
Noise power associated with uplink transmission	-90 dBm
Average transmission power/channel of ground base station	35.75 dBm (3.76 W)
Average transmission power/channel of UAV	35.68 dBm (3.70 W)
Subcarrier spacing (KHz)	60
Sampling frequency (MHz)	983.04
Antenna configuration	$(2, 2, 2) \times 8$
Signal-to-noise ratio (dB)	-10 to 10

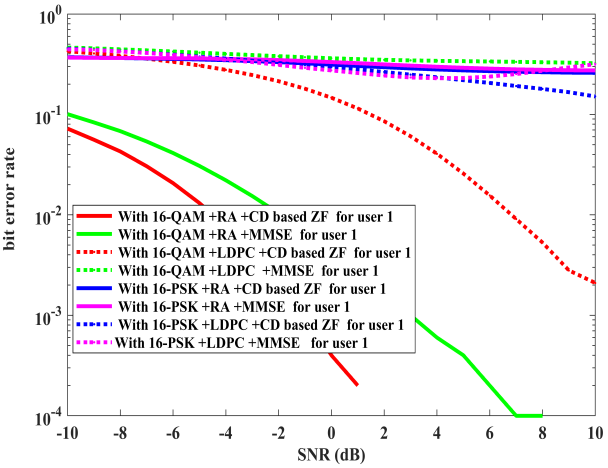

FIGURE 3. BER performance of considered system utilizing various channel coding, higher order digital modulation and signal detection techniques for user 1.

The presented BER simulation results in Figure 3 through Figure 5 show the impact of implementing various channel coding under two higher order digital modulation schemes(16-QAM and 16-PSK) and two signal detection techniques (CD based ZF and MMSE) on system performance for each of the three users.

In all cases, the simulated full-duplex UAV based zero-padded OFDM system shows relatively better performance at 16-QAM in comparison with 16-PSK utilizing RA channel coding and CD based zero forcing signal detection techniques.

It can be observed from graphical illustrations presented in Figure 3 for user 1 that the performance of the simulated system shows better performance under RA channel coding technique adopting CD based ZF signal detection and worst performance under LDPC channel coding technique adopting MMSE signal detection in 16-QAM higher order digital modulation respectively.

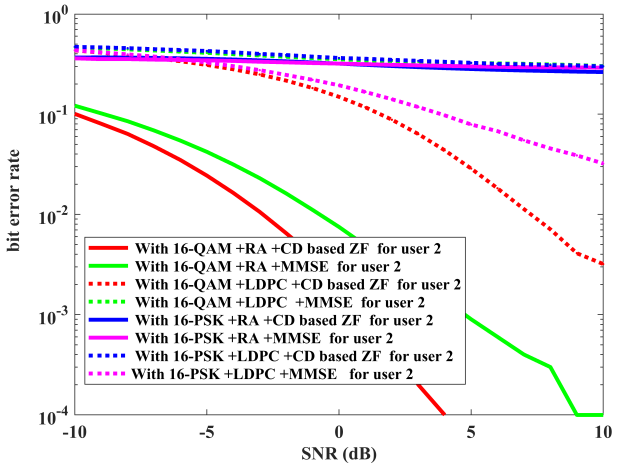

FIGURE 4. BER performance of considered system with utilization of various channel coding, higher order digital modulation and signal detection techniques for user 2.

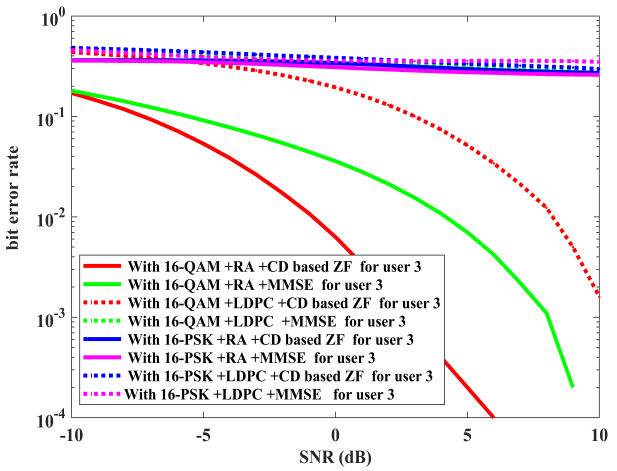

FIGURE 5. BER performance of considered system with utilization of various channel coding, higher order digital modulation and signal detection techniques for user 3.

Figure 3 shows that the estimated BERs are found to have values of 0.0004, 0.0044 and 0.1467 in case of RA channel coding adopting CD based ZF signal detection, RA channel coding adopting MMSE signal detection and LDPC channel coding adopting CD based ZF signal detection under 16-QAM higher order digital modulation respectively for identical SNR value of 0 dB. For such specifically investigated case, overall improvement of 10.414 dB and 25.644 dB are achieved in the system utilizing RA channel coding adopting CD based ZF signal detection as compared to RA channel coding adopting MMSE signal detection and LDPC channel coding adopting CD based ZF signal detection for 16-QAM. In case of 16-PSK digital modulation, the overall performance under all the parameters is not satisfactory in comparison with 16-QAM digital modulation. However, critical observation of the system depicts that the BER values of 0.3367 and 0.2059 are achieved in case of LDPC channel coding adopting MMSE signal detection and LDPC channel coding adopting CD based ZF at customarily considered SNR value of 6 dB under 16-QAM and 16-PSK higher order digital modulation technique respectively. Thus it signifies system performance improvement of 2.136 dB in LDPC channel coding adopting CD based ZF under 16-PSK digital modulation.

Figure 4 is related to user 2, where it is seen that the evaluated BERs under 16-QAM are found to have values of 0.0006, 0.0032 and 0.0882 for RA channel coding adopting CD based ZF signal detection, RA channel coding adopting MMSE signal detection and LDPC channel coding adopting CD based ZF signal detection respectively at customarily considered SNR value of 2 dB. These parameters are clearly suggesting overall improvement of 7.269 dB and 21.673 dB in the system for RA channel coding adopting CD based ZF signal detection in comparison with RA channel coding adopting MMSE signal detection and LDPC channel coding adopting CD based ZF signal detection technique respectively. With 16-PSK, it is observable that the overall trend of BERs for the case of RA channel coding adopting CD based ZF signal detection and RA channel coding adopting MMSE signal detection are almost identical in nature. At customarily accepted 5 dB SNR, evaluated BERs are 0.2821, 0.3, 0.3256 and 0.0789 for RA channel coding adopting CD based ZF signal detection, RA channel coding adopting MMSE signal detection, LDPC channel coding adopting CD based ZF signal detection and LDPC channel coding adopting MMSE signal detection under 16-PSK. These parameters signify overall improvement of 5.533 dB, 5.800 dB and 6.156 dB in the system for LDPC channel coding adopting MMSE signal detection in comparison with RA channel coding adopting CD based ZF signal detection, RA channel coding adopting MMSE signal detection and LDPC channel coding adopting CD based ZF signal detection respectively.

Figure 5 is applicable for user 3 and in such case, the simulated system provides worst BER performance as compared to system performance of other users. At customarily considered 5 dB SNR with 16-QAM, the evaluated BERs are 0.0002, 0.007 and 0.0516 for RA channel coding adopting CD based ZF signal detection, RA channel coding adopting MMSE signal detection and LDPC channel coding adopting CD based ZF signal detection respectively. These parameters are clearly illustrating an overall improvement of 15.441 dB and 24.116 dB as the system performance for the case of RA channel coding adopting CD based ZF signal detection in comparison with RA channel coding adopting MMSE signal detection and LDPC channel coding adopting CD based ZF signal detection technique respectively. In case of 16-PSK, the system performances are not well discriminated and also ratifying worst performance considering all other parameters.

In Figure 6, BER performances of the proposed system have been presented with and without application of WHT orthogonal technique. In such case, channel coding techniques have not been used merely to avoid its impact on BER performance. For a typically assumed scenario of identical signal and noise power (SNR = 0 dB), the evaluated BERs are (0.0728, 0.0832 and 0.1219) and (0.2325, 0.2328 and 0.2930)

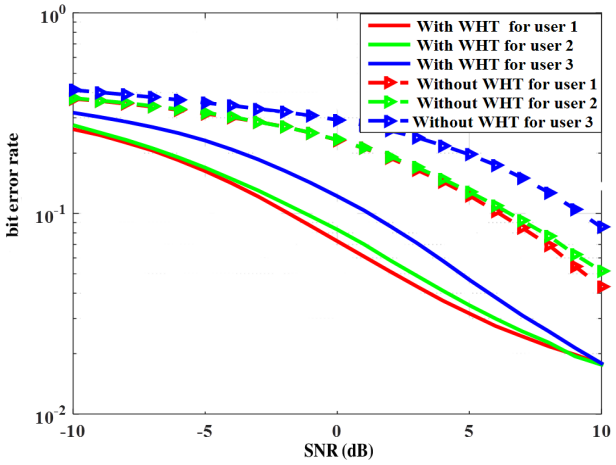

FIGURE 6. Impact of implementing WHT orthogonal technique in BER performance improvement of considered system.

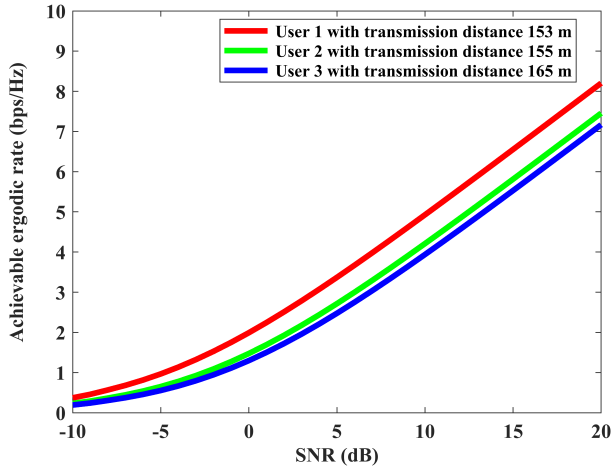

FIGURE 7. Estimated achievable ergodic rate of three users versus receive signal-to noise ratio with an average UAV transmission power of 3.7 W.

in case of implementing and non-implementing WHT orthogonal technique for user 1, user 2 and user 3 which are suggesting an overall improvement of 5.04 dB, 4.47 dB and 3.81 dB in the system performance.

In Figure 7, achievable user's ergodic information rates are provided. It is observable that the achievable ergodic rate increases almost linearly with increasing values of received signal-to-noise ratio (SNR) which indicates that the QR-decomposition based Zero forcing (ZF) Block Diagonalization (QR-ZF-BD) precoding scheme has facilitated inter-user interference and noise cancellation properly. For a typically assumed SNR value of 15 dB, the estimated achievable ergodic rate/ achievable ergodic spectral efficiency values of the three users are 6.55 bps/Hz, 5.82 bps/Hz and 5.53 bps/Hz respectively with an average achievable ergodic rate of 5.97 bps/Hz and achievable ergodic sum-rate of the proposed system is of 17.90 bps/Hz.

In Figure 8, ergodic secrecy rate curves are depicted for three users. Such estimated ergodic secrecy rate is mostly dominated by the quality of the Eavesdropper's wiretap

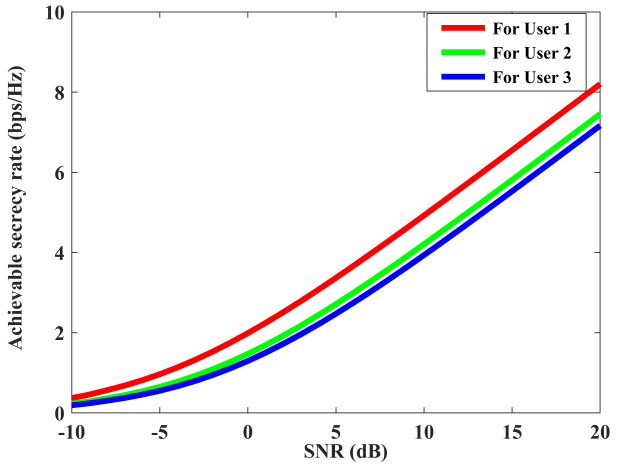

FIGURE 8. Estimated achievable secrecy rate of three users versus receive signal-to noise ratio with an average UAV transmission power of 3.7 W.

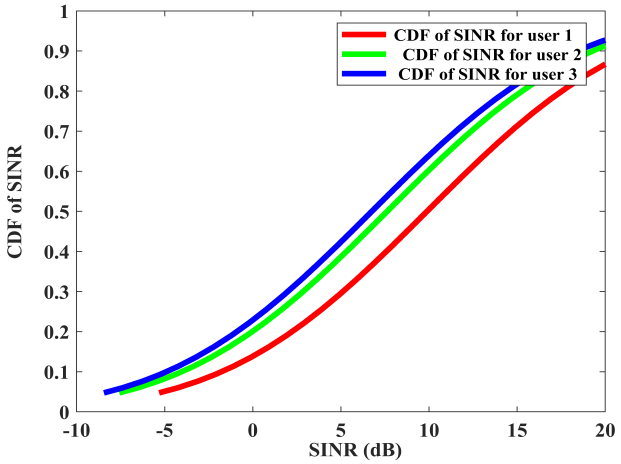

FIGURE 9. Cumulative Distribution Function (CDF) of the estimated Signal to Interference and Noise Ratio (SINR) for three users.

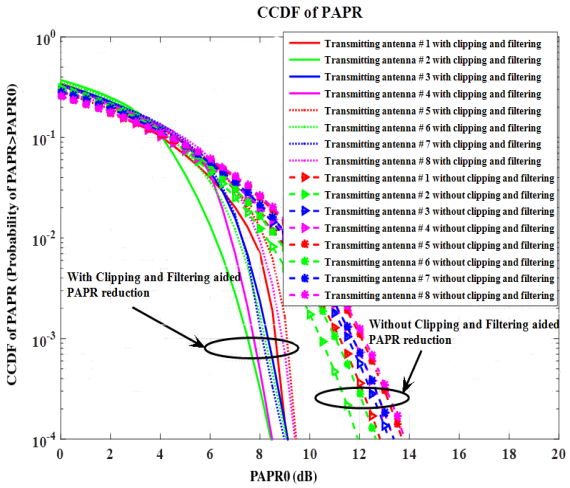

FIGURE 10. CCDFs of PAPR for considered system with and without utilization of Clipping and Filtering aided PAPR scheme at Ground base station.

channel. With adaptation of artificial noisy signal, it is observable that at low SNR regime, ergodic secrecy rate is improved viz. the achievable ergodic rate of each user

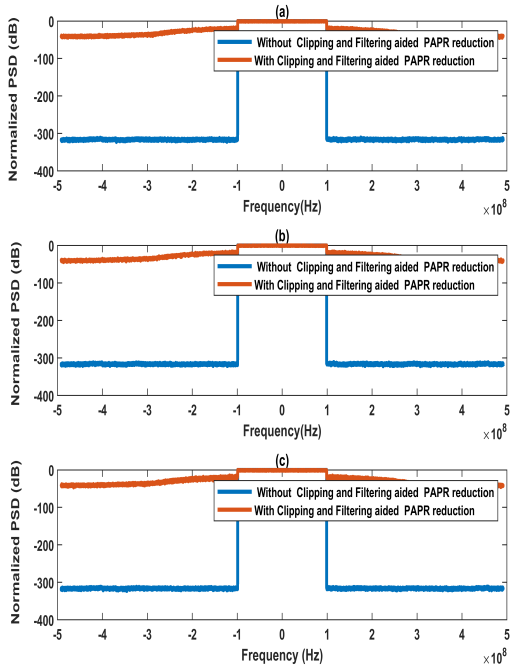

FIGURE 11. Power spectral density of considered system implementing Clipping and filtering aided PAPR reduction, 16-QAM higher order digital modulation, RA Channel coding and WHT schemes for; (a) User 1, (b) User 2, (c) User 3.

is higher as compared to achievable ergodic rate of the eavesdropper with identical number of receive antennas of all the users and eavesdropper.

Figure 9 illustrates the computed cumulative distribution function (CDF) of the signal to interference and noise ratio (SINR) received by the different users. From Figure 9, it is noticeable that the SINR outage probability distributions are quite different under varying user locations from the serving UAV base station. In a typically assumed probability value of 50%, user 1 achieves an SINR value of 9.91 dB, user 2 achieves an SINR value of 7.65 dB, user 3 achieves an SINR value of 6.78 dB viz, all the three users in the proposed system can establish communication with SINR value ranging from 9.91dB to 6.78 dB.

In Figure 10, complementary cumulative distribution functions (CCDFs) are representing the probability of signal's envelope of different transmitting antenna channels above threshold level. These are used to enumerate the performance of minimizing PAPR. With implementation of non-iterative clipping and filtering aided scheme for PAPR minimization targeting PAPR of 6 dB, it is observable from Figure 10 that utilization of such scheme is capable of enhancing PAPR reduction performance. For a typically assumed 1×10^{-4} CCDF of PAPR value, the ground transmitting base station channels have PAPR (greater than the threshold) values ranging from 8.5 dB to 9.5 dB in case of clipping and filtering aided PAPR scheme implementation. On the other hand, without its utilization PAPR values increase and range from 12.5 dB to 14.0 dB which ratifies a PAPR gain of 4.25 dB. At 6 dB PAPR (greater than the threshold), its

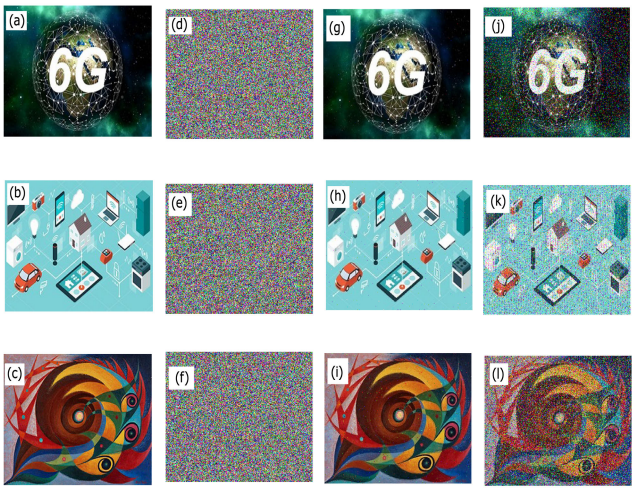

FIGURE 12. Transmitted color image for; (a) user 1, (b) user 2, (c) user 3. Encrypted color image for; (d) user 1, (e) user 2, (f) user 3. Retrieved color image at SNR value of 0 dB for; (g) user 1, (h) user 2, (i) user 3. Retrieved color image at SNR value of −10 dB for; (j) user 1, (k) user 2, (l) user 3.

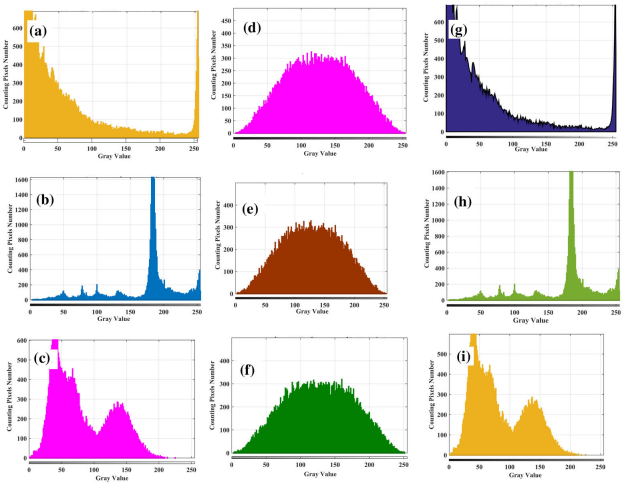

FIGURE 13. Histogram of transmitted color to gray converted image for; (a) user 1, (b) user 2, (c) user 3. Histogram of encrypted color to gray converted image for; (d) user 1, (e) user 2, (f) user 3. Histogram of retrieved color to gray converted image for; (g) user 1, (h) user 2, (i) user 3.

CCDF probability level was found to confine within 1-6%. The estimated values of PAPR at the transmitting channels without implementation of Clipping and Filtering aided PAPR scheme are 16.0451 14.7634 16.4029 17.0598 16.7874 15.7673 16.5736 16.7907 dB with an average PAPR value of 16.27 dB. In case of utilizing clipping and filtering aided PAPR scheme, the estimated PAPR values achieve to the values of 11.5103 11.2737 10.6322 10.7693 10.6229 10.8013 10.2552 10.6113 dB with an average PAPR value of 10.81 dB.

It is quite obvious from Figure 11 that the OOB power reduction of 318.52 dB, 315.99 dB and 319.26 dB are achieved corresponding to non-implementing clipping and filtering aided PAPR reduction techniques for user 1, user 2 and user 3. The OOB power reduction degrades and achieves to the values of 40.21 dB, 39.36 dB and 41.07 dB in case of implementing clipping and filtering aided PAPR reduction and such executable operation makes significant improvement of PAPR reduction.

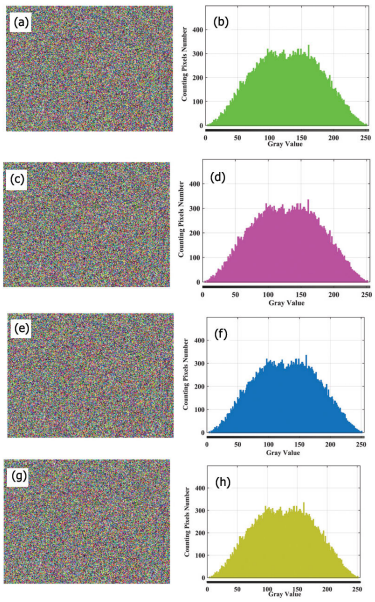

FIGURE 14. (a) Artificial noise contaminated transmitted color image for Eavesdropper, (b) Histogram of transmitted image, (c) Retrieved image at 0 dB SNR, (d) Histogram of retrieved image at 0 dB, (e) Retrieved image at 10 dB SNR, (f) Histogram of retrieved image at 10 dB, (g) Retrieved image at −10 dB SNR, (h) Histogram of retrieved image at −10 dB.

Figure 12 illustrates transmitted and encrypted images as well as the retrieved images of three different users at 0 dB and −10 dB SNR value. It is clearly observed from the figure that retrieved images of each user at 0 dB SNR value is acceptable than the images retrieved at −10 dB SNR value.

The histograms illustrated in Figure 13 are visibly signifying the distribution of pixel values of color to gray converted transmitted, encrypted and retrieved images. In terms of Figure 13, it is quite clear that the retrieved histograms get resemblance as to original color images in case of all three users.

From Figure 14, it is quite evident that due to implementation of PLS with an addition of artificially generated noisy signal and WHT technique integrated with QR-decomposition based Zero forcing (ZF) Block Diagonalization (QR-ZF-BD) precoding, proposed anti-eavesdropping system mitigate passive eavesdropping properly and prevents stealing of information of three users transmitted over unsecured public network. The study is developed on an assumption that the eavesdropper is quite aware of the block diagonalization, WHT, channel coding and signal detection techniques assigned for him/her.

In Figure 15, a comparative analysis has been made in terms of bit error rate (BER) against signal-to-noise ratio (SNR) between the proposed full-duplex UAV based zero-padded secured OFDM system and OFDM/NOMA aided multicarrier signaling technique implemented systems. The authors of [31] utilized complex-valued deep neural networks in order to study the performance of deep complex convolutional network (DCCN) based CP OFDM system in terms of BER for low order to higher order digital modulation under AWGN channel.

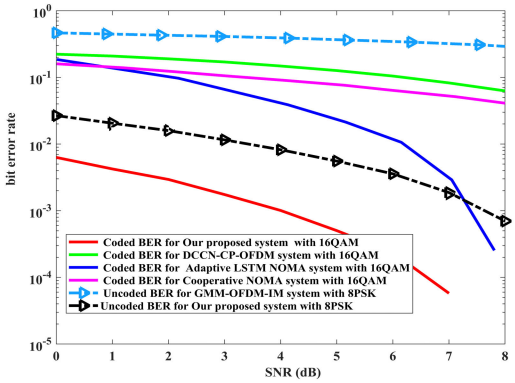

FIGURE 15. Bit error rate (BER) against signal-to-noise ratio (SNR) for the proposed system with multi-carrier coded and uncoded signaling technique implemented systems.

The authors of [32] investigated the performance of the NOMA system considering outage probability, capacity, BER and user power allocation accuracy. In their proposed system, long-short term memory (LSTM) neural network with adaptive channel coding and digital modulation was introduced. From the works of [33], it has been observed that the authors developed an architecture based on novel hybrid-cascaded deep neural network (DNN) with a view to optimizing cooperative NOMA system in a holistic manner. In Figure 15, illustrated BER results are applicable for 16-QAM digital modulation with coded BER. It is very much noteworthy from the presented results that the proposed system outperforms all the other OFDM/NOMA systems. For a typically assumed SNR value of 5 dB, the evaluated BER values are 0.0002, 0.0150, 0.0750 and 0.1298 in case of Zero padded OFDM, LSTM NOMA, Cooperative NOMA and DCCN-CP OFDM system. These parameters are clearly indicating an overall performance improvement of 18.75 dB, 25.74 dB and 28.12 dB for the case of the proposed system in comparison with channel encoded BER performance of the other three systems. Furthermore, in case of uncoded BER performance, the estimated BER values are 0.3593 and 0.0040 for index modulation aided multiple-mode OFDM (GMM-OFDM-IM) system and the proposed zero padded OFDM system with 8PSK digital modulation respectively which ratifies a system performance improvement of 19.77dB and of course the applicability of channel coding would undoubtedly improve BER performance.

IV. CONCLUSION

In this paper, a framework to design transceiver for full-duplex UAV-assisted downlink cooperative zero-padded OFDM system at mmWave is presented. In the proposed system, UAV is combined with terrestrial cellular network in addition of PLS. Decode-and-forward strategy is espoused by the UAV considering sudden blockages from high storied building in urban areas. The simulation outcome proves the effectiveness of the proposed system with improved BER performance under higher order digital modulation at reasonably acceptable PAPR as compared to the systems associated with

OFDM/NOMA utilizing index modulation. Besides, it has been observed that the proposed system also outperforms the system incorporating OFDM with index modulation in terms of the spectral efficiency and secrecy rate. Based on the results, the implementation of RA channel coding with CD based ZF signal detection technique provided better performance for the case of all users. In addition, the received color images of all users become totally unrecognizable to the eavesdropper that also ratifies properly addressed security issue of the proposed system. In the future, multiple UAVs can be considered along with more improved technique for the physical layer encryption in case of OFDM-based massive MIMO scheme.

REFERENCES

[1] S. Iranmanesh, F. S. Abkenar, R. Raad, and A. Jamalipour, "Improving throughput of 5G cellular networks via 3D placement optimization of logistics drones," *IEEE Trans. Veh. Technol.*, vol. 70, no. 2, pp. 1448–1460, Feb. 2021.

[2] S. Iranmanesh, R. Raad, M. S. Raheel, F. Tubbal, and T. Jan, "Novel DTN mobility-driven routing in autonomous drone logistics networks," *IEEE Access*, vol. 8, pp. 13661–13673, 2020, doi: 10.1109/ACCESS.2019.2959275.

[3] S. Iranmanesh and R. Raad, "A novel data forwarding strategy for a drone delay tolerant network with range extension," *Electronics*, vol. 8, no. 6, p. 659, Jun. 2019.

[4] G. Mu, "Joint beamforming and power allocation for wireless powered UAV-assisted cooperative NOMA systems," *EURASIP J. Wireless Commun. Netw.*, vol. 2020, no. 1, pp. 1–14, Dec. 2020.

[5] W. Saad, M. Bennis, M. Mozaffari, and X. Lin, *Wireless Communications and Networking for Unmanned Aerial Vehicles*. Cambridge, U.K.: Cambridge Univ. Press, 2020.

[6] S. Huang, M. Xiao, and H. V. Poor, "On the physical layer security of millimeter wave NOMA networks," *IEEE Trans. Veh. Technol.*, vol. 69, no. 10, pp. 11697–11711, Oct. 2020.

[7] Y. Huang, J. Zhang, and M. Xiao, "Constant envelope hybrid precoding for directional millimeter-wave communications," *IEEE J. Sel. Areas Commun.*, vol. 36, no. 4, pp. 845–859, Apr. 2018.

[8] A. A. Zaidi, R. Baldemair, V. Molés-Cases, N. He, K. Werner, and A. Cedergren, "OFDM numerology design for 5G new radio to support IoT, eMBB, and MBSFN," *IEEE Commun. Standards Mag.*, vol. 2, no. 2, pp. 78–83, Jun. 2018.

[9] *5G; NR; Physical Layer; General Description*, document TS 38.201, 3GPP, Version 15.0.0, Sep. 2018.

[10] S. Tanangsanakool, P. Reangsuntea, K. Mori, and P. Boonsrimuang, "Low complexity equalization method for ZP-OFDM under highly mobile environments," in *Proc. 22nd Int. Conf. Adv. Commun. Technol. (ICACT)*, Phoenix Park, South Korea, Feb. 2020, pp. 12–17.

[11] M. Wen, Q. Li, E. Basar, and W. Zhang, "Generalized multiple-mode OFDM with index modulation," *IEEE Trans. Wireless Commun.*, vol. 17, no. 10, pp. 6531–6543, Oct. 2018.

[12] J. Li, S. Dang, M. Wen, X.-Q. Jiang, Y. Peng, and H. Hai, "Layered orthogonal frequency division multiplexing with index modulation," *IEEE Syst. J.*, vol. 13, no. 4, pp. 3793–3802, Dec. 2019.

[13] M. Wen, B. Ye, E. Basar, Q. Li, and F. Ji, "Enhanced orthogonal frequency division multiplexing with index modulation," *IEEE Trans. Wireless Commun.*, vol. 16, no. 7, pp. 4786–4801, Jul. 2017.

[14] N. Senadhira, S. Durrani, X. Zhou, N. Yang, and M. Ding, "Impact of UAV trajectory on NOMA-assisted cellular-connected UAV networks," in *Proc. IEEE Int. Conf. Commun. (ICC)*, Dublin, Ireland, Jun. 2020, pp. 1–7.

[15] X. Tan, S. Su, X. Guo, and X. Sun, "Application of MIMO-OFDM technology in UAV communication network," in *Proc. 2nd World Symp. Artif. Intell. (WSAI)*, Guangzhou, China, Jun. 2020, pp. 1–4.

[16] S. Kumari, K. K. Srinivas, and P. Kumar, "Channel and carrier frequency offset equalization for OFDM based UAV communications using deep learning," *IEEE Commun. Lett.*, vol. 25, no. 3, pp. 850–853, Mar. 2021.

[17] M. Dua, A. Suthar, A. Garg, and V. Garg, "An ILM-cosine transform-based improved approach to image encryption," *Complex Intell. Syst.*, vol. 7, no. 1, pp. 327–343, Feb. 2021.

[18] M. Sadeghzadeh, M. Maleki, and M. Salehi, "Large-scale analysis of regularized block diagonalization precoding for physical layer security of multi-user MIMO wireless networks," *IEEE Trans. Veh. Technol.*, vol. 68, no. 6, pp. 5820–5834, Jun. 2019.

[19] Y. Chen, W. Feng, and G. Zheng, "Optimum placement of UAV as relays," *IEEE Commun. Lett.*, vol. 22, no. 2, pp. 248–251, Feb. 2018.

[20] G. A. Vitetta, D. P. Taylor, G. Colavolpe, F. Pancaldi, and P. A. Martin, *Wireless Communications: Algorithmic Techniques*. Hoboken, NJ, USA: Wiley, 2013.

[21] Y. Jiang, *A Practical Guide to Error-Control Coding Using MATLAB*. Norwood, MA, USA: Artech House, 2010.

[22] T. Rappaport, *Wireless Communications: Principles and Practice*, vol. 2. Upper Saddle River, NJ, USA: Prentice-Hall, 1996.

[23] A. A. C. A. Jayathilake, A. A. I. Perera, and M. A. P. Chamikara, "Discrete Walsh–Hadamard transform in signal processing," *Int. J. Res. Inf. Technol*, vol. 1, pp. 80–89, Jan. 2013.

[24] S. Gökceli, T. Levanen, T. Riihonen, J. Yli-Kaakinen, A. Brihuega, M. Turunen, M. Renfors, and M. Valkama, "Novel iterative clipping and error filtering methods for efficient PAPR reduction in 5G and beyond," *IEEE Open J. Commun. Soc.*, vol. 2, pp. 48–66, 2021.

[25] J. Wu, S. Fang, L. Li, and Y. Yang, "QR decomposition and gram Schmidt orthogonalization based low-complexity multi-user MIMO precoding," in *Proc. 10th Int. Conf. Wireless Commun., Netw. Mobile Comput. (WiCOM)*, Beijing, China, 2014, pp. 26–28.

[26] R. Gangarajaiah, H. Prabhu, O. Edfors, and L. Liu, "A Cholesky decomposition based massive MIMO uplink detector with adaptive interpolation," in *Proc. IEEE Int. Symp. Circuits Syst. (ISCAS)*, Baltimore, MD, USA, May 2017, pp. 1–4.

[27] Y. S. Cho, J. Kim, W. Y. Yang, and C. G. Kang, *MIMO-OFDM Wireless Communications With MATLAB*. Hoboken, NJ, USA: Wiley, 2010.

[28] W. Tan, S. Jin, J. Wang, and Y. Huang, "Achievable sum-rate analysis for massive MIMO systems with different array configurations," in *Proc. IEEE Wireless Commun. Netw. Conf. (WCNC)*, New Orleans, LA, USA, Mar. 2015, pp. 316–321.

[29] S. J. Maeng, Y. Yapıcı, I. Guvenç, H. Dai, and A. Bhuyan, "Precoder design for mmWave UAV communications with physical layer security," in *Proc. IEEE 21st Int. Workshop Signal Process. Adv. Wireless Commun. (SPAWC)*, Atlanta, GA, USA, May 2020, pp. 1–5.

[30] W. Tan, S. Jin, C.-K. Wen, and T. Jiang, "Spectral efficiency of multi-user millimeter wave systems under single path with uniform rectangular arrays," *EURASIP J. Wireless Commun. Netw.*, vol. 2017, no. 1, pp. 1–13, Dec. 2017.

[31] Z. Zhao, M. C. Vuran, F. Guo, and S. D. Scott, "Deep-waveform: A learned OFDM receiver based on deep complex-valued convolutional networks," 2018, *arXiv:1810.07181*. [Online]. Available: http://arxiv.org/abs/1810.07181

[32] M. AbdelMoniem, S. M. Gasser, M. S. El-Mahallawy, M.W. Fakhr, and A. Soliman, "Enhanced NOMA system using adaptive coding and modulation based on LSTM neural network channel estimation," *Appl. Sci.*, vol. 9, no. 15, p. 3022, Jul. 2019.

[33] Y. Lu, P. Cheng, Z. Chen, W. H. Mow, Y. Li, and B. Vucetic, "Deep multi-task learning for cooperative NOMA: System design and principles," *IEEE J. Sel. Areas Commun.*, vol. 39, no. 1, pp. 61–78, Jan. 2021.

JOARDER JAFOR SADIQUE received the B.Sc. (Hons.) and M.Sc. degrees in applied physics and electronic engineering (currently named as electrical and electronic engineering) from the University of Rajshahi, Rajshahi, Bangladesh, in 2010 and 2011, respectively. He was a Faculty Member with the Electrical and Electronic Engineering Department, University of Information Technology and Sciences (UITS), Dhaka, Bangladesh, from May 2013 to March 2014. From March 2014 to October 2017, he was a Lecturer with the Department of Electrical and Electronic Engineering, Begum Rokeya University, Rangpur, Bangladesh, where has been serving as an Assistant Professor since October 2017. His main research interests include 5G/6G compatible mmWave hybrid precoded communications, the Internet of Things (IoT), unmanned aerial vehicle (UAV), cooperative communications, CoMP in MIMO OFDM/OFDMA, channel equalization, and modern channel coding techniques.

SHAIKH ENAYET ULLAH received the B.Sc. (Hons.) and M.Sc. degrees in applied physics and electronics from the University of Rajshahi, Rajshahi, Bangladesh, in 1981 and 1982, respectively, and the Ph.D. degree from Jahangirnagar University, Dhaka, Bangladesh, in 2000. He was the Head of the Department of Information and Communication Engineering, University of Rajshahi, from January 2009 to January 2012. He was also the Head of the Department of Applied Physics and Electronic Engineering (currently named as Electrical and Electronic Engineering), University of Rajshahi, from October 2013 to February 2015. He is currently a Professor of electrical and electronic engineering with the University of Rajshahi. His current research interests include 5G compatible mmWave communications, advanced radio access technology-based: NOMA, filter-bank multicarrier (FBMC), index modulation aided OFDM, bi-orthogonal frequency division multiplexing, generalized frequency division multiplexing (GFDM), universal frequency division multiplexing (UFDM), multi-level differential chaos shift keying (DCSK), massive MIMO communications, free space optical communications, cooperative communications, COMP in MIMO OFDM/OFDMA, fading and interference mitigation, and channel equalization and coding.

MD. RABIUL ISLAM (Senior Member, IEEE) received the Ph.D. degree in electrical engineering from the University of Technology Sydney (UTS), Sydney, Australia, in 2014.

He was appointed as a Lecturer at RUET, in 2005, where he was promoted to a Full Professor in 2017. In early 2018, he joined the School of Electrical, Computer, and Telecommunications Engineering (SECTE), University of Wollongong (UOW), Wollongong, Australia. He has authored or coauthored more than 200 articles, including 54 IEEE TRANSACTIONS/IEEE Journal articles. He has written or edited five technical books published by Springer and Taylor & Francis. His research interests include power electronic converters, renewable energy technologies, power quality, electrical machines, electric vehicles, and smart grid. He has received several Best Paper Awards, including two Best Paper recognitions from IEEE TRANSACTIONS ON ENERGY CONVERSION in 2020. He has received several funding from Government and Industries, including Australian Government ARC Discovery Project 2020 titled ''A Next Generation Smart Solid-State Transformer for Power Grid Applications.'' He has served as a Guest Editor for IEEE TRANSACTIONS ON ENERGY CONVERSION, IEEE TRANSACTIONS ON APPLIED SUPERCONDUCTIVITY, and *IET Electric Power Applications*. He has been serving as an Editor for IEEE TRANSACTIONS ON ENERGY CONVERSION and IEEE POWER ENGINEERING LETTERS and an Associate Editor for IEEE ACCESS.

RAAD RAAD (Member, IEEE) received the B.Eng. degree (Hons.) in electrical engineering from the University of Wollongong, Wollongong, Australia, in 1997, and the master's degree from the Switched Networks Research Centre, University of Wollongong. He received the Australian Postgraduate Award (APA) that was matched by Telstra Research Laboratories (TRL). A further scholarship was awarded from the Motorola Australian Research Centre (MARC) in the later part of his degree. He went on to complete his Ph.D. degree titled ''Neuro-Fuzzy Logic Admission Control in Cellular Mobile Networks'' in 2006. Since 2004, he has been with the School of Electrical, Computer and Telecommunications Engineering, University of Wollongong, where he serves as the Deputy Head of the School. His current research interests include wireless communications, CubeSat, the IoT, and antenna design.

ABBAS Z. KOUZANI (Member, IEEE) received the B.Sc. degree in computer engineering from the Sharif University of Technology, Iran, the M.Eng.Sc. degree in electrical and electronic engineering from The University of Adelaide, Australia, and the Ph.D. degree in electrical and electronic engineering from Flinders University, Australia. He was a Lecturer with the School of Engineering, Deakin University, Australia, and then a Senior Lecturer with the School of Electrical Engineering and Computer Science, University of Newcastle, Australia. He is currently a Professor with the School of Engineering, Deakin University. He is also the Director of the Advanced Integrated Microsystems (AIM) Research Group, Deakin University. He provides research leadership in embedded, connected, and low-power devices, circuits, and instruments that incorporate sensing, actuation, control, wireless transmission, networking and the IoT, data acquisition/storage/analysis, AI, energy harvesting, power management, and fabrication for tackling research questions relating to a variety of disciplines, including healthcare, ecology, mining, infrastructure, automotive, manufacturing, energy, utilities, and agriculture. He has produced more than 370 publications, including one book, 17 book chapters, 180 journal articles, and 181 fully refereed conference papers. He has three patents and two pending patents. He has been involved in more than $15 million research grants, and has managed projects and delivered research solutions to more than 25 Australian and International companies. He has supervised 24 research fellows/assistants, and produced 28 Ph.D. and six Masters by Research completions. He is also involved in supervision of 12 Ph.D. students. He received several awards, including the Outstanding Contribution to Scholarly Publication Award from the School of Engineering, Deakin University, in 2019.

M. A. PARVEZ MAHMUD received the B.Sc. degree in electrical and electronic engineering and the M.Eng. degree in mechatronics engineering. After the successful completion of his Ph.D. degree with multiple awards, he has worked as a Postdoctoral Research Associate and an Academic with the School of Engineering, Macquarie University, Sydney. He has worked as a Lecturer with the World University of Bangladesh (WUB) for more than two years and a Researcher with the Korea Institute of Machinery and Materials (KIMM) for about three years. He is currently an Alfred Deakin Postdoctoral Research Fellow with Deakin University. He is also involved in the supervision of eight Ph.D. students at Deakin University. He is a key member of the Advanced Integrated Microsystems (AIM) Research Group, Deakin University. His research interests include energy sustainability, secure energy trading, microgrid control and economic optimization, machine learning, data science, and micro/nanoscaled technologies for sensing and energy harvesting. He accumulated experience and expertise in machine learning, life cycle assessment, sustainability and economic analysis, materials engineering, microfabrication, and nanostructured energy materials to facilitate technological translation from the laboratory to real-world applications for the better society. He has produced more than 110 publications, including one authored book, nine book chapters, 49 journal articles, and 29 fully refereed conference papers. He was involved in teaching engineering subjects in the electrical, biomedical, and mechatronics engineering courses at the School of Engineering, Macquarie University, for more than two years. Apart from this, he is actively involved with different professional organizations, including Engineers Australia and IEEE. He received several awards, including the Macquarie University Highly Commended Excellence in Higher Degree Research Award in 2019.